



Effect of Convection, Internal Heat Source, and Solar Radiation on the Stress Analysis of a Rotating Functionally Graded Smart Disk

Mahdi Saadatfar¹ · Mohammad Amin Babazadeh¹ · Mojtaba Babaelahi¹

Received: 25 June 2023 / Accepted: 26 October 2023 / Published online: 10 March 2024
© The Author(s), under exclusive licence to Shiraz University 2024

Abstract

In this study, stresses and deformations of a rotating functionally graded magneto-electro-elastic (FGMEE) disk with non-uniform thickness considering internal heat generation, convection, and radiation heat transfer were investigated. The power-law function of the radial coordinate was considered for the properties of the material. Also, the heat conduction and convection coefficients are functions of temperature and radius. The heat transfer equation was derived considering thermal gradient, convection thermal boundary, heat source, and solar radiation. The differential transformation method (DTM) was used for solving the obtained nonlinear differential equation of heat transfer. Then, the equilibrium equation of the disk was derived and solved analytically. So, the radial stress, hoop stress, radial deformation, electric and magnetic potential, electric displacement, and magnetic induction can be obtained. Finally, some numerical examples were presented to examine the effects of the heat source, convection heat transfer, temperature dependency, solar radiation, inhomogeneity index, and angular velocity on the stress, deformation, electric displacement, and magnetic induction of the disk. The results show the tensile radial stress, deformation, electric displacement, and magnetic induction decrease for higher values of source power and solar flux intensity, while changes for the higher values of convection coefficient and thermal conductivity are opposite. Also, using a non-uniform thickness disk with an outer thickness smaller than the inner thickness can reduce the displacement and electromagnetic potentials.

Keywords Rotating disk · Functionally graded magneto-electro-elastic · Stress analysis · Variable thickness · Solar radiation · Heat source

List of Symbols

r_o	Exterior radius (m)	Ω	Thickness profile coefficient
r_i	Interior radius (m)	y_0	Thickness profile coefficient
T	Temperature (K)	a_i	Temperature function coefficients
T_a	Ambient air temperature (K)	γ	Inhomogeneity index
T_b	Inner temperature (K)	a	Convection coefficient
T_o	Outer temperature (K)	b	Convection coefficient
k_0	Thermal conductivity (W/mK)	θ	Dimensionless temperature
β	Conduction heat transfer coefficient	η	Dimensionless radius
ω	Angular speed (Rad/s)	σ_r	Radial stress (Pa)
h_0	Convection heat transfer coefficient (W/m ² K)	σ_θ	Hoop stress (Pa)
G_s	Solar flux intensity (W/m ²)	σ_z	Normal stress (Pa)
α_s	Absorption coefficient of solar radiation	u_r	Radial displacement (m)
ε	Emission coefficient of solar radiation	c_{ij}	Elastic constants (GPa)
ψ	Magnetic potential (A)	D_r	Electric displacement (C/m ²)
		e_{ij}	Piezoelectric coefficients (C/m ²)
		q_{ij}	Piezomagnetic coefficients (N/Am)
		ε_{ij}	Electromagnetic coefficients (Ns/VC)
		β_{ij}	Dielectric coefficients (C ² /Nm ²)
		α_i	Thermal expansion coefficients (1/K)

✉ Mahdi Saadatfar
m.saadatfar@gmail.com; m.saadatfar@qom.ac.ir

¹ Department of Mechanical Engineering, Faculty of Engineering, University of Qom, Qom, Iran

ρ	Density (kg/m^3)
ϕ	Electric potential (W/A)
B_r	Magnetic induction (T)
λ_i	Thermal modulus ($\text{N/m}^2\text{K}$)
σ	Stefan–Boltzmann constant
$H\{t\}$	DTM transformation coefficients
d_{ij}	Magnetic coefficients (Ns^2/C^2)
ε_i	Components of strain
E_r	Components of electric field
p_i	Pyroelectric coefficients ($\text{C}^2/\text{m}^2\text{K}$)
m_i	Pyromagnetic coefficients (N/AmK)

1 Introduction

Today's, new materials such as functionally graded materials (FGMs), smart materials, smart composites, and nanofluids are the focus of many articles (Ahmad et al. 2019; Ahmad et al. 2021a, b; Ahmad 2023). FGM is one of these that has attracted a lot of attention in recent years and many articles have been published in this field (Singh and Harsha 2020; Alibeigloo 2021; Saadatfar et al. 2023a, b; Saadatfar et al. 2023a, b). Functionally graded magneto-electro-elastic material is a type of smart composite structure that can convert the energy from mechanical to magnetic or electric type and vice versa. These materials have many potential applications in important industries, such as aerospace, turbine rotor designing, magnetic storage, smart structures, and many other fields (Chang et al. 2020; Saadatfar and Zarandi 2020a, b; Saadatfar 2021a, b; Ly et al. 2022).

Several reported articles investigate the stresses and deformation of rotating disks. Sahni and Sahni (2015) examined a rotating FGM disk with variable thickness and considered external pressure. Thermoelastic analysis of an FGM rotating disk has been done by Dai and Dai (2016). In this analysis, the thickness and angular speed of the disk have been considered to be variable. Hosseini et al. (2016) analyzed the stress of rotating FGM nanodisks with variable thickness profiles. Rattan et al. (2016) investigated the creep behavior of an isotropic disk made of composite. In this work, the thermal residual stress has been considered. Dai et al. (2017) investigated a rotating functionally graded piezoelectric disk located in a hygrothermal field. Creep analysis of an FGM rotating disk considering the Tresca criteria has been done by Khanna et al. (2017). The results of this analysis have been compared to von Mises criteria results. Thawait et al. (2017) used the element-based material grading for the elastic analysis of an FGM rotating disk with non-constant thickness. Bose and Rattan (2018) investigated the influence of thermal gradation on the creep behavior of an FGM rotating disk. Designing FGM rotating disks by weight optimization has been done by Khorsand and Tang (2018).

The designed disks have been examined under thermomechanical loads. Considering the rule of mixture, the stress and deformation of an FGM rotating disk have been analyzed by Madan et al. (2018). Hayat et al. (2018) examined the flow of a nanofluid due to a rotating disk. In this analysis, the influences of chemical reaction and heat generation have been considered and the final ordinary differential equation has been solved using homotopy analysis method. Hosseini et al. (2019) studied rotating FGM micro/nanodisks considering a variable thickness profile. Li et al. (2019) studied the transient response of a rotating turbine disk experimentally. In this examination, the thermal loading management strategy has been used. Madan et al. (2019) investigated the limit of angular speed of a rotating disk made of functionally graded material using temperature-dependent/independent mechanical properties. The deformation of a rotating composite disk due to the thermal gradient has been analyzed by Kaur et al. (2020). Saadatfar and Zarandi (2020a, b) examined the mechanical behaviors of a rotating annular plate made of FGPM considering variable thickness. Sondhi et al. (2020) analyzed the stress and deformation of an FGM disk with variable thickness considering orthotropic structure and rotation. Ahmad et al. (2021a, b) modeled the effect of the magnetic field on a rotating disk flow considering heat transfer. The effects of angular deceleration on the behaviors of multilayer disks made of functionally graded material have been investigated by Eldeeb et al. (2021). Responses of an FGPM cylinder considering hygrothermal loading have been examined by Saadatfar (2021a, b). Saber and Abd_Elsalam (2022) presented a theoretical model for the investigation of the performance of FGM rotating disks.

There are many works on stress analysis of FGMEE structures in the literature. Akbarzadeh and Chen (2012) analyzed FGMEE rotating cylinders resting on an elastic foundation. The considered cylinders were analyzed under hygrothermal loading. Gupta and Singh (2016) modeled the creep of an FGM rotating disk mathematically considering the variable thickness. Dai and Dai (2017) analyzed a rotating FGMEE disk in thermal environment. Dai et al. (2019) examined a porous FGMEE disk in hygrothermal environment and analyzed its mechanical behaviors. Ebrahimi et al. (2019) studied the effect of porosity on dynamic characteristics of the heterogeneous FGMEE plates. Investigation of influences of porosity, thickness profile, and rotational acceleration on the behaviors of an FGMEE rotating disk has been done by Saadatfar et al. (2021). The analyzed disk was located in a constant magnetic field. Zhang et al. (2022) studied the static and dynamic behaviors of FGMEE shells and plates. Zhou et al. (2022) analyzed the static behaviors of inhomogeneous FGMEE plates in thermal environment. The element-free Galerkin method has been used in this analysis.

The literature review shows stress analysis of rotating variable thickness FGMEE disks with a convection heat

transfer, an internal heat source, and solar radiation for the case that heat convection and conduction coefficients are dependent on temperature and radius has not been analyzed. So, the novelties of this article are considering conduction and convection heat transfer coefficients as functions of temperature and radius, and considering the effects of heat transfer including the conduction, convection, solar radiation, and internal heat source. The power-law function of the radius was considered for material properties. The obtained nonlinear differential equation was solved using DTM. Then, the equilibrium equation was derived and solved analytically to achieve stresses, displacement, electric and magnetic potential distributions.

2 Thermal Equations

In this article, a variable thickness FGMEE disk has been considered as shown in Fig. 1. The rotation of the disk is around its Z-axis. Four types of heat transfer phenomena are considered: conduction, convection, internal heat generation, and solar radiation. Regarding symmetry and plane stress conditions, nonzero components of displacement and temperature are functions of radius. A power-law function of the radius has been used for the thickness profile of the disk:

$$h(r) = y_0 r^{-\Omega}. \tag{1}$$

2.1 Thermal Equations Derivation

In thermal analysis, there are four methods for heat exchange, which are heat conduction, heat convection, internal heat generation, and solar radiation. It is important to mention that convective and conductive heat transfer coefficients change with temperature and radius. According to the energy balance equation, we have (Incropera et al. 1996):

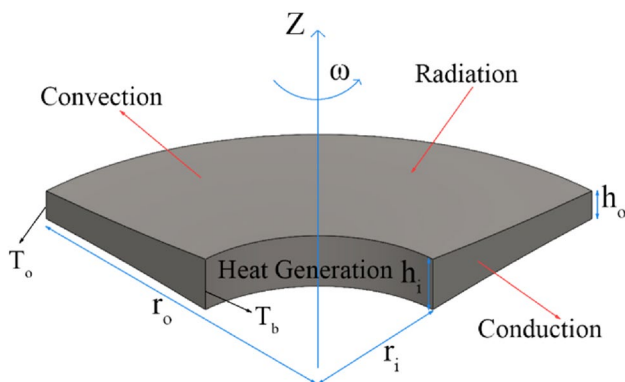


Fig. 1 Schematic of the rotating FGMEE disk

$$\frac{d}{dr} \left(K A_c \frac{dT}{dr} \right) dr - h(T - T_a) dA_s + \alpha_s G_s dA_s - \varepsilon \sigma (T^4 - T_a^4) dA_s + \dot{q} dV = 0. \tag{2}$$

where

$$K = k_0 r^\gamma (1 + \beta \theta), \tag{3}$$

$$h = h_0 \theta^\Gamma (a + b \omega r), \tag{4}$$

$$\dot{q} = q_0 (1 + e_0 \theta). \tag{5}$$

For the simplification, the following variable change is considered:

$$\theta = \frac{T - T_b}{T_a - T_b}, \tag{6}$$

$$\eta = \frac{r - r_i}{r_o - r_i}. \tag{7}$$

where T_b and T_a are the inner radius temperature of the disk and ambient air temperature, respectively. The expression $(\alpha_s G_s dA_s)$ indicates the amount of solar radiation received by the disk. Also, the expression $(\varepsilon \sigma (T^4 - T_a^4) dA_s)$ refers to the reflected radiation of the disk. Using the introduced parameters and simplifying, Eq. (2) can be written as:

$$\begin{aligned} & \frac{(T_a - T_b)}{(r_o - r_i)^2} \cdot \frac{d}{d\eta} \left\{ y_0 (1 + \beta \theta) (r_i + \eta (r_o - r_i))^{\gamma+1-\Omega} \frac{d\theta}{d\eta} \right\} \\ & - \frac{h_0}{k_0} \theta^\Gamma (\theta - 1) (T_a - T_b) (r_i + \eta (r_o - r_i)) (a + b \omega (r_i + \eta (r_o - r_i))) \\ & + (r_i + \eta (r_o - r_i)) \left(\frac{\alpha_s G_s}{k_0} - \frac{\varepsilon \sigma}{k_0} ((\theta (T_a - T_b) + T_b)^4 - T_a^4) \right) \\ & + \frac{q_0 y_0}{k_0} (r_i + \eta (r_o - r_i))^{1-\Omega} (1 + e_0 \theta) = 0. \end{aligned} \tag{8}$$

The obtained differential equation (Eq. (8)) is a second-order type. Therefore, it will be important to use two boundary conditions:

$$r = r_i : \eta = 0 \rightarrow T = T_b : \theta = 0, \tag{9}$$

$$r = r_o : \eta = 1 \rightarrow T = T_o : (T_a - T_b) \theta + T_b = T_o. \tag{10}$$

According to the introduced boundary conditions, the internal and external temperature of the disk will be constant.

2.2 Solution of Nonlinear Thermal Differential Equation

The well-known DTM was used for solving the nonlinear heat transfer differential equation in Eq. (8). This method creates a polynomial analytical approach for differential

equations. DTM is an iterative procedure for gaining analytical Taylor series solutions for differential equations. The necessary functions of this method are presented in Appendix. Now, the final differential transformation of Eq. (8) can be expressed as:

$$\begin{aligned}
 & \left\{ \sum_{x=0}^k \sum_{v=0}^x H_1[v](\beta\theta[x-v] + \delta(x-v))(k-x+1)\theta[k-x+1] \right\} \\
 & + \left\{ \sum_{x=0}^k \sum_{v=0}^x H_2[v]((x-v+1)\theta[x-v+1])(k-x+1)\theta[k-x+1] \right\} \\
 & - \left\{ \sum_{x=0}^k \sum_{v=0}^x H_3[v](\beta\theta[x-v] + \delta(x-v))(k-x+1)\theta[k-x+1] \right\} \\
 & + \left\{ \sum_{x=0}^k \sum_{v=0}^x H_4[v](\beta\theta[x-v] + \delta(x-v))(k-x+1)(k-x+2)\theta[k-x+2] \right\} \\
 & - \left\{ \sum_{x=0}^k \sum_{v=0}^x \sum_{r=0}^v \sum_{w=0}^r H_7[w]\theta[r-w]\theta[v-r]\theta[x-v](\theta[k-x] - \delta(k-x)) \right\} \\
 & + \{H_5[k]\} \\
 & - \left\{ \sum_{x=0}^k \sum_{v=0}^x \sum_{r=0}^v \sum_{w=0}^r H_6[w]((T_a - T_b)\theta[r-w] + T_b\delta(r-w))((T_a - T_b)\theta[v-r] + T_b\delta(v-r)) \right. \\
 & \left. ((T_a - T_b)\theta[x-v] + T_b\delta(x-v))((T_a - T_b)\theta[k-x] + T_b\delta(k-x)) \right\} \\
 & + \{T_a^4 H_6[k]\} + \left\{ \sum_{x=0}^k H_8[x](\delta(k-x) + e_0\theta[k-x]) \right\} = 0.
 \end{aligned} \tag{11}$$

where

$$\begin{aligned}
 H_1[t] &= y_0 \frac{T_a - T_b}{(r_o - r_i)} (\gamma + 1) (r_i + t(r_o - r_i))^{\gamma - \Omega}, \\
 H_2[t] &= y_0 \beta \frac{T_a - T_b}{(r_o - r_i)^2} (r_i + t(r_o - r_i))^{\gamma - \Omega + 1}, \\
 H_3[t] &= y_0 \Omega \frac{T_a - T_b}{(r_o - r_i)} (r_i + t(r_o - r_i))^{\gamma - \Omega}, \\
 H_4[t] &= y_0 \frac{T_a - T_b}{(r_o - r_i)^2} (r_i + t(r_o - r_i))^{\gamma - \Omega + 1}, \\
 H_5[t] &= \frac{\alpha_s G_s}{k_0} (r_i + t(r_o - r_i)), \\
 H_6[t] &= \frac{\varepsilon \sigma}{k_0} (r_i + t(r_o - r_i)), \\
 H_7[t] &= \frac{h_0}{k_0} (T_a - T_b) (r_i + t(r_o - r_i)) (a + b\omega(r_i + t(r_o - r_i))), \\
 H_8[t] &= \frac{y_0 q_0}{k_0} (r_i + t(r_o - r_i))^{1 - \Omega}.
 \end{aligned} \tag{12}$$

where δ is the Dirac delta function and $x, k, w, v,$ and r are the sigma boundaries used in the DTM method. The transformed boundary conditions can be expressed as:

$$\begin{aligned}
 \theta[0] &= 0, \\
 \theta[1] &= \mu_0.
 \end{aligned} \tag{13}$$

In the next step, the coefficients of the main dimensionless temperature function will be obtained using the iterative procedure; such as:

$$\begin{aligned}
 \theta[2] &= \frac{-1}{2r_i^{\gamma+1}} \{ \beta r_i^{\gamma+1} \mu^2 + r_i^{\gamma+1} \Omega \mu - r_i^\gamma r_o \Omega \mu - r_i^{\gamma+1} \gamma \mu \\
 & + r_i^\gamma r_o \gamma \mu - r_i^{\gamma+1} \mu + r_i^\gamma r_o \mu + \frac{(r_o - r_i)^2}{(T_a - T_b) y_0} \frac{\varepsilon \sigma}{k_0} T_a^4 r_i^{\Omega+1} \\
 & - \frac{(r_o - r_i)^2}{(T_a - T_b) y_0} \frac{\varepsilon \sigma}{k_0} T_b^4 r_i^{\Omega+1} + \frac{(r_o - r_i)^2}{(T_a - T_b)} \frac{q_0}{k_0} r_i \\
 & + \frac{(r_o - r_i)^2}{(T_a - T_b) y_0} \frac{\alpha_s G_s}{k_0} r_i^{\Omega+1} \}.
 \end{aligned} \tag{14}$$

Finally, we have:

$$\theta(\eta) = \sum_{i=1}^U \theta[i] \eta^i = \theta_0 + \theta_1 \eta + \theta_2 \eta^2 + \theta_3 \eta^3 + \theta_4 \eta^4 + \theta_5 \eta^5. \tag{15}$$

Now, substituting θ and η , the temperature function was derived as:

$$T(r) = a_0 + a_1 r + a_2 r^2 + a_3 r^3 + a_4 r^4 + a_5 r^5. \tag{16}$$

3 Stress Field Equations

3.1 Basic Equations

Stress–strain relations of FGMEE disk can be expressed as (Saadatfar 2019; Saadatfar et al. 2021):

$$\sigma_r = c_{11}\epsilon_{rr} + c_{12}\epsilon_{\theta\theta} + c_{13}\epsilon_{zz} - e_{11}E_r - q_{11}H_r - \lambda_1 T, \quad (17)$$

$$\sigma_\theta = c_{12}\epsilon_{rr} + c_{22}\epsilon_{\theta\theta} + c_{23}\epsilon_{zz} - e_{12}E_r - q_{12}H_r - \lambda_2 T, \quad (18)$$

$$\sigma_z = c_{13}\epsilon_{rr} + c_{23}\epsilon_{\theta\theta} + c_{33}\epsilon_{zz} - e_{13}E_r - q_{13}H_r - \lambda_3 T, \quad (19)$$

$$D_r = e_{11}\epsilon_{rr} + e_{12}\epsilon_{\theta\theta} + e_{13}\epsilon_{zz} + \beta_{11}E_r + \varepsilon_{11}H_r + p_1 T, \quad (20)$$

$$B_r = q_{11}\epsilon_{rr} + q_{12}\epsilon_{\theta\theta} + q_{13}\epsilon_{zz} + \varepsilon_{11}E_r + d_{11}H_r + m_1 T. \quad (21)$$

Considering the plane stress condition, we have:

$$\sigma_z = 0 \Rightarrow \epsilon_{zz} = -\frac{c_{13}}{c_{33}}\epsilon_{rr} - \frac{c_{23}}{c_{33}}\epsilon_{\theta\theta} + \frac{e_{13}}{c_{33}}E_r + \frac{q_{13}}{c_{33}}H_r + \frac{\lambda_3}{c_{33}}T. \quad (22)$$

Replacing Eq. (22) in Eqs. (17), (18), (20), and (21) yields to:

$$\sigma_r = c'_{11}\frac{\partial u}{\partial r} + c'_{12}\frac{u}{r} + e'_{11}\frac{\partial \phi}{\partial r} + q'_{11}\frac{\partial \psi}{\partial r} - \lambda'_1 T, \quad (23)$$

$$\sigma_\theta = c'_{12}\frac{\partial u}{\partial r} + c'_{22}\frac{u}{r} + e'_{12}\frac{\partial \phi}{\partial r} + q'_{12}\frac{\partial \psi}{\partial r} - \lambda'_2 T, \quad (24)$$

$$D_r = e'_{11}\frac{\partial u}{\partial r} + e'_{12}\frac{u}{r} - \beta'_{11}\frac{\partial \phi}{\partial r} - \varepsilon'_{11}\frac{\partial \psi}{\partial r} + p'_1 T, \quad (25)$$

$$B_r = q'_{11}\frac{\partial u}{\partial r} + q'_{12}\frac{u}{r} - \varepsilon'_{11}\frac{\partial \phi}{\partial r} - d'_{11}\frac{\partial \psi}{\partial r} + m'_1 T. \quad (26)$$

where

$$\begin{aligned} c'_{11} &= c_{11} - \frac{c_{13}^2}{c_{33}}, & c'_{12} &= c_{12} - \frac{c_{13}c_{23}}{c_{33}}, & c'_{22} &= c_{22} - \frac{c_{23}^2}{c_{33}}, \\ e'_{11} &= e_{11} - \frac{c_{13}e_{13}}{c_{33}}, & e'_{12} &= e_{12} - \frac{c_{23}e_{13}}{c_{33}}, & q'_{11} &= q_{11} - \frac{c_{13}q_{13}}{c_{33}}, \\ q'_{12} &= q_{12} - \frac{c_{23}q_{13}}{c_{33}}, & \lambda'_1 &= \lambda_1 - \frac{c_{13}\lambda_3}{c_{33}}, & \lambda'_2 &= \lambda_2 - \frac{c_{23}\lambda_3}{c_{33}}, \\ m'_1 &= m_1 + \frac{\lambda_3 q_{13}}{c_{33}}, & d'_{11} &= d_{11} + \frac{q_{13}^2}{c_{33}}, & \beta'_{11} &= \beta_{11} + \frac{e_{13}^2}{c_{33}}, \\ \varepsilon'_{11} &= \varepsilon_{11} + \frac{e_{13}q_{13}}{c_{33}}, & p'_1 &= p_1 + \frac{e_{13}\lambda_3}{c_{33}}. \end{aligned} \quad (27)$$

For simplicity, all of the material properties are supposed to change based on a power-law function:

$$P = \bar{P}r^\gamma. \quad (28)$$

where \bar{P} is the material constant. Finally, the nonzero terms of the equilibrium equation of the rotating FGMEE disk are (Saadatfar 2021a, b):

$$\frac{\partial(h(r)\sigma_r)}{\partial r} + h(r)\frac{(\sigma_r - \sigma_\theta)}{r} + h(r)pr\omega^2 = 0. \quad (29)$$

Also, the electrostatic and magnetostatic equations are in the following form:

$$\frac{\partial(h(r)D_r)}{\partial r} + \frac{h(r)D_r}{r} = 0, \quad (30)$$

$$\frac{\partial(h(r)B_r)}{\partial r} + \frac{h(r)B_r}{r} = 0. \quad (31)$$

The solution of Eqs. (30) and (31) can be introduced as:

$$D_r = \frac{A_1}{r^{-\Omega+1}} = e'_{11}\frac{\partial u}{\partial r} + e'_{12}\frac{u}{r} - \beta'_{11}\frac{\partial \phi}{\partial r} - \varepsilon'_{11}\frac{\partial \psi}{\partial r} + p'_1 T, \quad (32)$$

$$B_r = \frac{A_2}{r^{-\Omega+1}} = q'_{11}\frac{\partial u}{\partial r} + q'_{12}\frac{u}{r} - \varepsilon'_{11}\frac{\partial \phi}{\partial r} - d'_{11}\frac{\partial \psi}{\partial r} + m'_1 T. \quad (33)$$

where A_1 and A_2 are unknown constants. According to Eqs. (32) and (33), we can recognize the electric and magnetic potential equations as:

$$\frac{\partial \phi(r)}{\partial r} = L_1\frac{\partial u}{\partial r} + L_2\frac{u}{r} + L_3\frac{A_2}{r^{\gamma-\Omega+1}} - L_5\frac{A_1}{r^{\gamma-\Omega+1}} + L_4 T, \quad (34)$$

$$\frac{\partial \psi(r)}{\partial r} = P_1\frac{\partial u}{\partial r} + P_2\frac{u}{r} + P_3\frac{A_1}{r^{\gamma-\Omega+1}} - P_5\frac{A_2}{r^{\gamma-\Omega+1}} + P_4 T. \quad (35)$$

where

$$\begin{aligned} L_1 &= \frac{e'_{11}d'_{11} - q'_{11}e'_{11}}{d'_{11}\beta'_{11} - \varepsilon'^2_{11}}, & L_2 &= \frac{e'_{12}d'_{11} - q'_{12}e'_{11}}{d'_{11}\beta'_{11} - \varepsilon'^2_{11}}, & L_3 &= \frac{\varepsilon'_{11}}{d'_{11}\beta'_{11} - \varepsilon'^2_{11}}, \\ L_4 &= \frac{p'_1 d'_{11} - m'_1 e'_{11}}{d'_{11}\beta'_{11} - \varepsilon'^2_{11}}, & L_5 &= \frac{d'_{11}}{d'_{11}\beta'_{11} - \varepsilon'^2_{11}}, \\ P_1 &= \frac{q'_{11}\beta'_{11} - \varepsilon'_{11}e'_{11}}{d'_{11}\beta'_{11} - \varepsilon'^2_{11}}, & P_2 &= \frac{q'_{12}\beta'_{11} - \varepsilon'_{11}e'_{12}}{d'_{11}\beta'_{11} - \varepsilon'^2_{11}}, & P_3 &= \frac{\varepsilon'_{11}}{d'_{11}\beta'_{11} - \varepsilon'^2_{11}}, \\ P_4 &= \frac{m'_1\beta'_{11} - \varepsilon'_{11}p'_1}{d'_{11}\beta'_{11} - \varepsilon'^2_{11}}, & P_5 &= \frac{\beta'_{11}}{d'_{11}\beta'_{11} - \varepsilon'^2_{11}}. \end{aligned} \quad (36)$$

Using Eqs. (34) and (35), the stress equations become simpler:

$$\sigma_r = C_1 r^\gamma \frac{\partial u}{\partial r} + C_2 r^\gamma \frac{u}{r} + C_3 \frac{A_2}{r^{-\Omega+1}} + C_4 \frac{A_1}{r^{-\Omega+1}} + C_5 r^\gamma T - \lambda'_1 r^{2\gamma} T, \quad (37)$$

$$\sigma_{\theta} = E_1 r^{\gamma} \frac{\partial u}{\partial r} + E_2 r^{\gamma} \frac{u}{r} + E_3 \frac{A_2}{r^{-\Omega+1}} + E_4 \frac{A_1}{r^{-\Omega+1}} + E_5 r^{\gamma} T - \lambda_2' r^{2\gamma} T. \quad (38)$$

Substituting the temperature function (Eq. (16)) in Eq. (41) gives:

where:

$$C_1 = c'_{11} + e'_{11} L_1 + q'_{11} P_1, \quad C_2 = c'_{12} + e'_{11} L_2 + q'_{11} P_2, \quad C_3 = e'_{11} L_3 - q'_{11} P_5, \quad (39)$$

$$C_4 = q'_{11} P_3 - e'_{11} L_5, \quad C_5 = e'_{11} L_4 + q'_{11} P_4,$$

$$E_1 = c'_{12} + e'_{12} L_1 + q'_{12} P_1, \quad E_2 = c'_{22} + e'_{12} L_2 + q'_{12} P_2, \quad E_3 = e'_{12} L_3 - q'_{12} P_5, \quad (40)$$

$$E_4 = q'_{12} P_3 - e'_{12} L_5, \quad E_5 = e'_{12} L_4 + q'_{12} P_4.$$

Substituting Eqs. (37) and (38) in Eq. (29) yields:

$$\frac{\partial^2 u}{\partial r^2} + \frac{M_1}{r} \frac{\partial u}{\partial r} + \frac{M_2}{r^2} u = M_3 r^{\gamma-1} T + M_4 \frac{T}{r} + (M_6 r^{\gamma} - M_5) \frac{\partial T}{\partial r} + M_7 \frac{A_2}{r^{\gamma-\Omega+2}} + M_8 \frac{A_1}{r^{\gamma-\Omega+2}} - M_{13} r. \quad (41)$$

where:

$$\begin{aligned} \frac{\partial^2 u}{\partial r^2} + \frac{M_1}{r} \frac{\partial u}{\partial r} + \frac{M_2}{r^2} u = & (M_3 a_0) r^{\gamma-1} + (M_3 a_1 + M_6 a_1) r^{\gamma} \\ & + (M_3 a_2 + 2M_6 a_2) r^{\gamma+1} + (M_3 a_3 + 3M_6 a_3) r^{\gamma+2} + (M_3 a_4 + 4M_6 a_4) r^{\gamma+3} \\ & + (M_3 a_5 + 5M_6 a_5) r^{\gamma+4} + (M_4 a_0) r^{-1} + (M_4 a_1 - M_5 a_1) \\ & + (M_4 a_2 - 2M_5 a_2 - M_{13}) r + (M_4 a_3 - 3M_5 a_3) r^2 + (M_4 a_4 - 4M_5 a_4) r^3 \\ & + (M_4 a_5 - 5M_5 a_5) r^4 + M_7 \frac{A_2}{r^{\gamma-\Omega+2}} + M_8 \frac{A_1}{r^{\gamma-\Omega+2}}. \end{aligned} \quad (42)$$

We can write the solution of Eq. (43) in the following form:

$$u = B_1 r^{m_1} + B_2 r^{m_2} + B_3 r^{\gamma+1} + B_4 r^{\gamma+2} + B_5 r^{\gamma+3} + B_6 r^{\gamma+4} + B_7 r^{\gamma+5} + B_8 r^{\gamma+6} + B_9 r + B_{10} r^2 + B_{11} r^3 + B_{12} r^4 + B_{13} r^5 + B_{14} r^6 + B_{15} A_2 r^{-\gamma+\Omega} + B_{16} A_1 r^{-\gamma+\Omega}, \quad (44)$$

$$M_1 = \frac{(\gamma - \Omega + 1)C_1 + C_2 - E_1}{C_1}, \quad M_2 = \frac{(\gamma - \Omega)C_2 - E_2}{C_1}, \quad m_1 = \frac{1}{2} \left(-(M_1 - 1) + \sqrt{(M_1 - 1)^2 - 4M_2} \right), \quad (45)$$

$$M_3 = \frac{(2\gamma - \Omega + 1)\lambda_1' - \lambda_2'}{C_1}, \quad M_4 = \frac{E_5 - (\gamma - \Omega + 1)C_5}{C_1}, \quad M_5 = \frac{C_5}{C_1}, \quad m_2 = \frac{1}{2} \left(-(M_1 - 1) - \sqrt{(M_1 - 1)^2 - 4M_2} \right).$$

$$M_6 = \frac{\lambda_1'}{C_1}, \quad M_7 = \frac{E_3}{C_1}, \quad M_8 = \frac{E_4}{C_1}, \quad M_{13} = \frac{\rho\omega^2}{C_1}. \quad (42)$$

where:

Table 1 Material properties

Parameter	Value	Parameter	Value
$c_{11}(GPa)$	151	e_{13}	-2.5
c_{12}	53	$q_{11}(N/Am)$	345
c_{13}	120	q_{12}	265
c_{22}	151	q_{13}	265
c_{23}	120	$\rho(kg/m^3)$	7750
c_{33}	215	$\beta_{11}(C^2/Nm^2)$	5.8×10^{-9}
$\alpha_r(1/K)$	6×10^{-6}	$p_1(C^2/m^2K)$	-2.5×10^{-5}
α_θ	15×10^{-6}	$\epsilon_{11}(Ns/VC)$	2.82×10^{-9}
α_z	15×10^{-6}	$m_1(N/AmK)$	2.5×10^{-5}
$e_{11}(C/m^2)$	7.5	$d_{11}(Ns^2/C^2)$	95×10^{-6}
e_{12}	-2.5	$\mu(N/A^2)$	8.85×10^{-6}

Table 2 Used parameters for the FGMEE disk

Parameter	Value	Parameter	Value
r_o	0.25(m)	k_0	20(W/mK)
r_i	0.05(m)	h_0	25(W/m ² K)
T_a	278(K)	q_0	1(kW/m ³)
T_b	313(K)	a	4
T_o	288(K)	b	4
y_0	0.03	γ	0.6
Ω	0.25	Γ	3
ω	50π(Rad/s)	α_s	0.5
e_0	4	G_s	950(W/m ²)
β	4	ϵ	0.5

$$\begin{aligned}
 B_3 &= \frac{M_3 a_0}{(\gamma + 1)^2 + (M_1 - 1)(\gamma + 1) + M_2}, B_4 = \frac{(M_3 + M_6) a_1}{(\gamma + 2)^2 + (M_1 - 1)(\gamma + 2) + M_2}, \\
 B_5 &= \frac{(M_3 + 2M_6) a_2}{(\gamma + 3)^2 - (\gamma + 3) + M_1(\gamma + 3) + M_2}, B_6 = \frac{(M_3 + 3M_6) a_3}{(\gamma + 4)^2 + (M_1 - 1)(\gamma + 4) + M_2}, \\
 B_7 &= \frac{(M_3 + 4M_6) a_4}{(\gamma + 5)^2 - (\gamma + 5) + M_1(\gamma + 5) + M_2}, B_8 = \frac{(M_3 + 5M_6) a_5}{(\gamma + 6)^2 - (\gamma + 6) + M_1(\gamma + 6) + M_2}, \\
 B_9 &= \frac{M_4 a_0}{M_1 + M_2}, B_{10} = \frac{(M_4 - M_5) a_1}{2 + 2M_1 + M_2}, B_{11} = \frac{(M_4 - 2M_5) a_2 - M_{13}}{6 + 3M_1 + M_2}, \\
 B_{12} &= \frac{(M_4 - 3M_5) a_3}{12 + 4M_1 + M_2}, B_{13} = \frac{(M_4 - 4M_5) a_4}{20 + 5M_1 + M_2}, B_{14} = \frac{(M_4 - 5M_5) a_5}{30 + 6M_1 + M_2}, \\
 B_{15} &= \frac{M_7}{(1 - M_1)(\gamma - \Omega) + (-\gamma + \Omega)^2 + M_2}, B_{16} = \frac{M_8}{(1 - M_1)(\gamma - \Omega) + (-\gamma + \Omega)^2 + M_2}.
 \end{aligned} \tag{46}$$

B_1 and B_2 are unknown constants. By Substituting Eq. (44) in Eqs. (34) and (35), and integrating, the electric and magnetic potential functions can be obtained as:

$$\begin{aligned}
 \phi(r) &= \frac{(L_1 m_1 + L_2) B_1}{m_1} r^{m_1} + \frac{(L_1 m_2 + L_2) B_2}{m_2} r^{m_2} + \frac{(L_1(\gamma + 1) + L_2) B_3}{\gamma + 1} r^{\gamma+1} \\
 &+ \frac{(L_2 + L_1(\gamma + 2)) B_4}{\gamma + 2} r^{\gamma+2} + \frac{(L_2 + L_1(\gamma + 3)) B_5}{\gamma + 3} r^{\gamma+3} + \frac{(L_2 + L_1(\gamma + 4)) B_6}{\gamma + 4} r^{\gamma+4} \\
 &+ \frac{(L_2 + L_1(\gamma + 5)) B_7}{\gamma + 5} r^{\gamma+5} + \frac{(L_2 + L_1(\gamma + 6)) B_8}{\gamma + 6} r^{\gamma+6} + ((L_1 + L_2) B_9 + L_4 a_0) r \\
 &+ \frac{((2L_1 + L_2) B_{10} + L_4 a_1)}{2} r^2 + \frac{((3L_1 + L_2) B_{11} + L_4 a_2)}{3} r^3 + \frac{((4L_1 + L_2) B_{12} + L_4 a_3)}{4} r^4 + \frac{((5L_1 + L_2) B_{13} + L_4 a_4)}{5} r^5 \\
 &+ \frac{((6L_1 + L_2) B_{14} + L_4 a_5)}{6} r^6 - \frac{((L_2 - L_1(\gamma - \Omega)) B_{15} A_2 + (L_2 - L_1(\gamma - \Omega)) B_{16} A_1)}{\gamma - \Omega} r^{-\gamma+\Omega} \\
 &- \frac{L_3 A_2}{\gamma - \Omega} r^{-\gamma+\Omega} + \frac{L_5 A_1}{\gamma - \Omega} r^{-\gamma+\Omega} + Z_1,
 \end{aligned} \tag{47}$$

$$\begin{aligned}
 \psi(r) = & \frac{(P_1 m_1 + P_2) B_1}{m_1} r^{m_1} + \frac{(P_1 m_2 + P_2) B_2}{m_2} r^{m_2} + \frac{(P_1(\gamma + 1) + P_2) B_3}{\gamma + 1} r^{\gamma+1} \\
 & + \frac{(P_2 + P_1(\gamma + 2)) B_4}{\gamma + 2} r^{\gamma+2} + \frac{(P_2 + P_1(\gamma + 3)) B_5}{\gamma + 3} r^{\gamma+3} + \frac{(P_2 + P_1(\gamma + 4)) B_6}{\gamma + 4} r^{\gamma+4} \\
 & + \frac{(P_2 + P_1(\gamma + 5)) B_7}{\gamma + 5} r^{\gamma+5} + \frac{(P_2 + P_1(\gamma + 6)) B_8}{\gamma + 6} r^{\gamma+6} + ((P_1 + P_2) B_9 + P_4 a_0) r \\
 & + \frac{((2P_1 + P_2) B_{10} + P_4 a_1)}{2} r^2 + \frac{((3P_1 + P_2) B_{11} + P_4 a_2)}{3} r^3 \\
 & + \frac{((4P_1 + P_2) B_{12} + P_4 a_3)}{4} r^4 + \frac{((5P_1 + P_2) B_{13} + P_4 a_4)}{5} r^5 \\
 & + \frac{((6P_1 + P_2) B_{14} + P_4 a_5 + P_6 b_5)}{6} r^6 - \frac{((P_2 - P_1(\gamma - \Omega)) B_{15} A_2 + (P_2 - P_1(\gamma - \Omega)) B_{16} A_1)}{\gamma - \Omega} r^{-\gamma+\Omega} \\
 & - \frac{P_3 A_1}{\gamma - \Omega} r^{-\gamma+\Omega} + \frac{P_5 A_2}{\gamma - \Omega} r^{-\gamma+\Omega} + Z_2.
 \end{aligned} \tag{48}$$

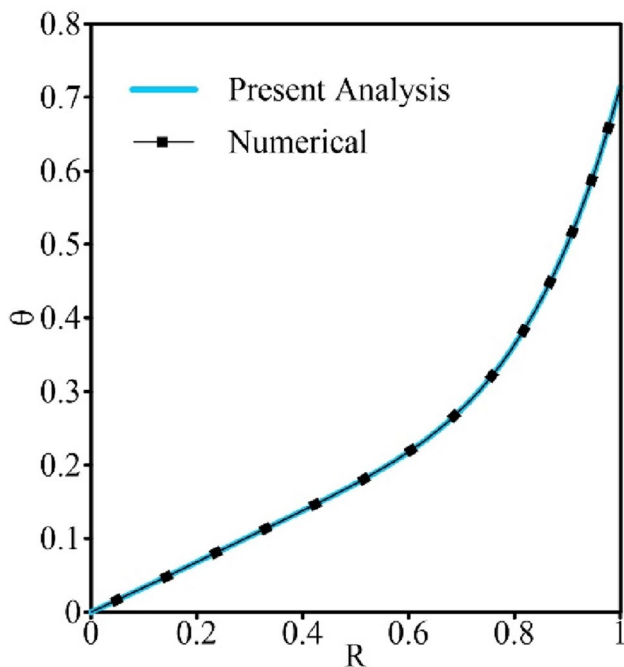


Fig. 2 Validation of results in thermal analysis

where, Z_1 and Z_2 are unknown coefficients. Since the radial displacement is known, the radial and hoop stresses can be calculated using Eqs. (44) in (37) and (38):

$$\begin{aligned}
 \sigma_r = & (C_1 m_1 + C_2) B_1 r^{\gamma+m_1-1} + (C_1 m_2 + C_2) B_2 r^{\gamma+m_2-1} \\
 & + (((\gamma + 1) C_1 + C_2) B_3 - \lambda'_1 a_0) r^{2\gamma} \\
 & + (((\gamma + 2) C_1 + C_2) B_4 - \lambda'_1 a_1) r^{2\gamma+1} \\
 & + (((\gamma + 3) C_1 + C_2) B_5 - \lambda'_1 a_2) r^{2\gamma+2} \\
 & + (((\gamma + 4) C_1 + C_2) B_6 - \lambda'_1 a_3) r^{2\gamma+3} \\
 & + (((\gamma + 5) C_1 + C_2) B_7 - \lambda'_1 a_4) r^{2\gamma+4} \\
 & + (((\gamma + 6) C_1 + C_2) B_8 - \lambda'_1 a_5) r^{2\gamma+5} + (B_9 (C_1 + C_2) + C_5 a_0) r^\gamma \\
 & + (B_{10} (2C_1 + C_2) + C_5 a_1) r^{\gamma+1} + (B_{11} (3C_1 + C_2) + C_5 a_2) r^{\gamma+2} \\
 & + (B_{12} (4C_1 + C_2) + C_5 a_3) r^{\gamma+3} + (B_{13} (5C_1 + C_2) + C_5 a_4) r^{\gamma+4} \\
 & + (B_{14} (6C_1 + C_2) + C_5 a_5) r^{\gamma+5} + ((C_2 - (\gamma - \Omega) C_1) A_2 B_{15} \\
 & + (C_2 - (\gamma - \Omega) C_1) A_1 B_{16}) r^{\Omega-1} \\
 & + C_3 \frac{A_2}{r^{-\Omega+1}} + C_4 \frac{A_1}{r^{-\Omega+1}},
 \end{aligned} \tag{49}$$

$$\begin{aligned}
 \sigma_\theta = & (E_1 m_1 + E_2) B_1 r^{\gamma+m_1-1} + (E_1 m_2 + E_2) B_2 r^{\gamma+m_2-1} + ((\gamma + 1)E_1 + E_2) B_3 - \lambda'_2 a_0) r^{2\gamma} \\
 & + ((\gamma + 2)E_1 + E_2) B_4 - \lambda'_2 a_1) r^{2\gamma+1} + ((\gamma + 3)E_1 + E_2) B_5 - \lambda'_2 a_2) r^{2\gamma+2} \\
 & + ((\gamma + 4)E_1 + E_2) B_6 - \lambda'_2 a_3) r^{2\gamma+3} + ((\gamma + 5)E_1 + E_2) B_7 - \lambda'_2 a_4) r^{2\gamma+4} \\
 & + ((\gamma + 6)E_1 + E_2) B_8 - \lambda'_2 a_5) r^{2\gamma+5} + (B_9(E_1 + E_2) + E_5 a_0) r^\gamma \\
 & + (B_{10}(2E_1 + E_2) + E_5 a_1) r^{\gamma+1} + (B_{11}(3E_1 + E_2) + E_5 a_2) r^{\gamma+2} \\
 & + (B_{12}(4E_1 + E_2) + E_5 a_3) r^{\gamma+3} + (B_{13}(5E_1 + E_2) + E_5 a_4) r^{\gamma+4} \\
 & + (B_{14}(6E_1 + E_2) + E_5 a_5) r^{\gamma+5} + ((E_2 - (\gamma - \Omega)E_1) A_2 B_{15} + (E_2 - (\gamma - \Omega)E_1) A_1 B_{16}) r^{\Omega-1} \\
 & + E_3 \frac{A_2}{r^{-\Omega+1}} + E_4 \frac{A_1}{r^{-\Omega+1}}.
 \end{aligned} \tag{50}$$

So, there are six unknown coefficients ($B_1, B_2, A_1, A_2, Z_1, Z_2$) that can be evaluated using the mechanical, electrical, and magnetic boundary conditions. Here, the boundary conditions are considered as:

$$\begin{aligned}
 r = r_i & \Rightarrow \sigma_r = 0, \quad \phi = \phi_i, \quad \psi = \psi_i, \\
 r = r_o & \Rightarrow \sigma_r = 0, \quad \phi = \phi_o, \quad \psi = \psi_o.
 \end{aligned} \tag{51}$$

4 Results and Discussion

Several numerical examples were considered in this part to disclose the effects of different parameters on the distribution of stresses, displacement, electric and magnetic potentials, and temperature. The used material constants are given in Table 1. Otherwise is states, the used parameters in the numerical

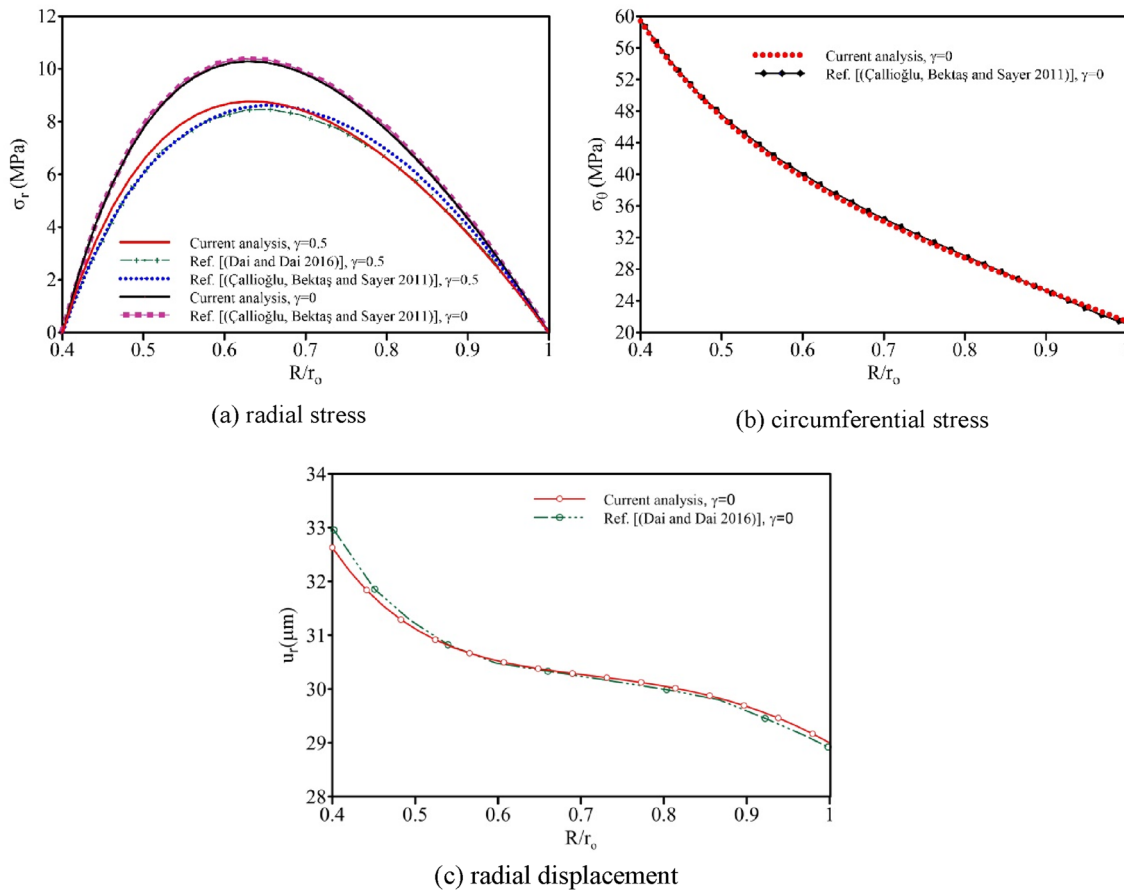
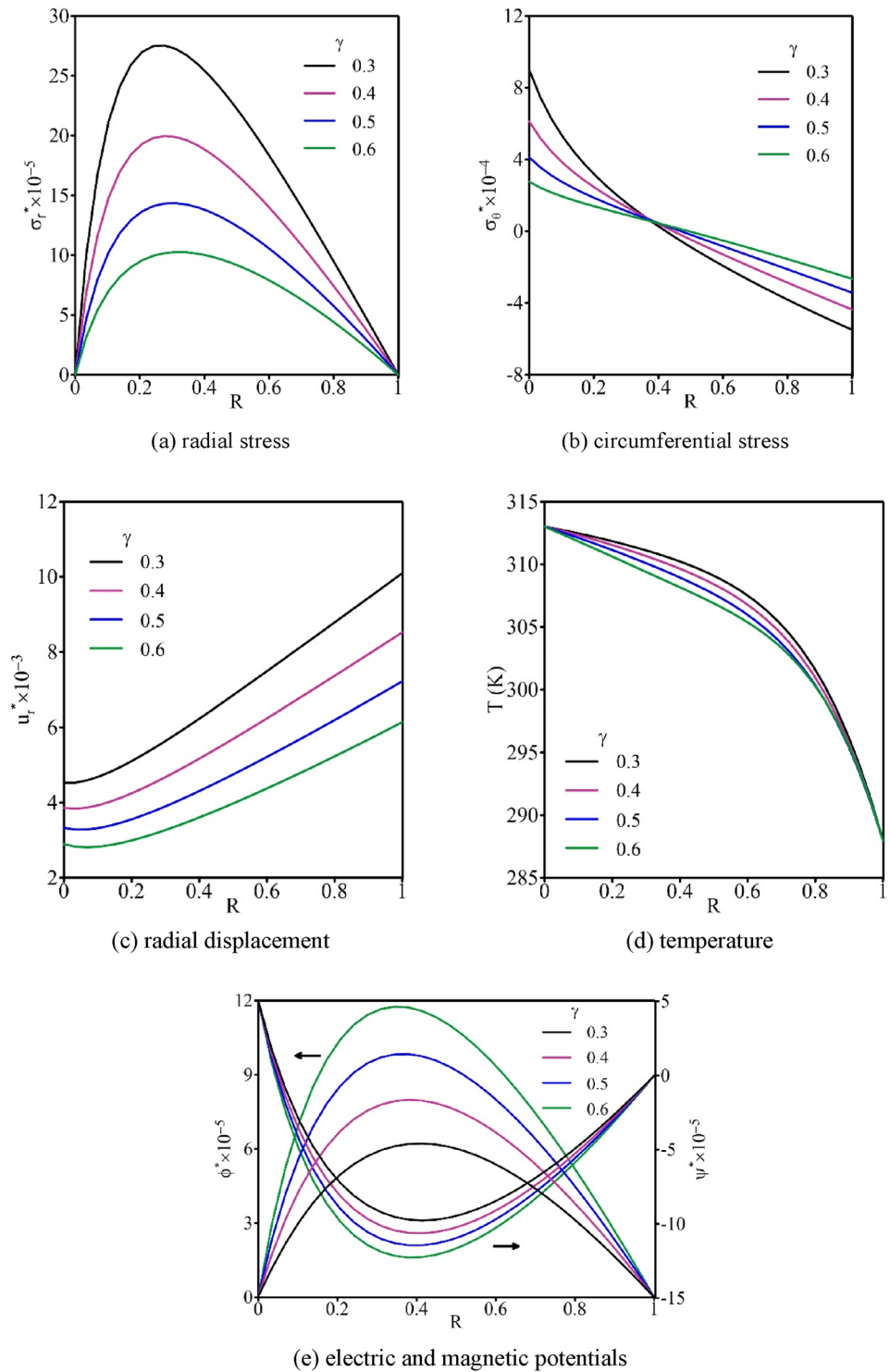


Fig. 3 Validation of the stress and deformation results

Fig. 4 Effect of the inhomogeneity index



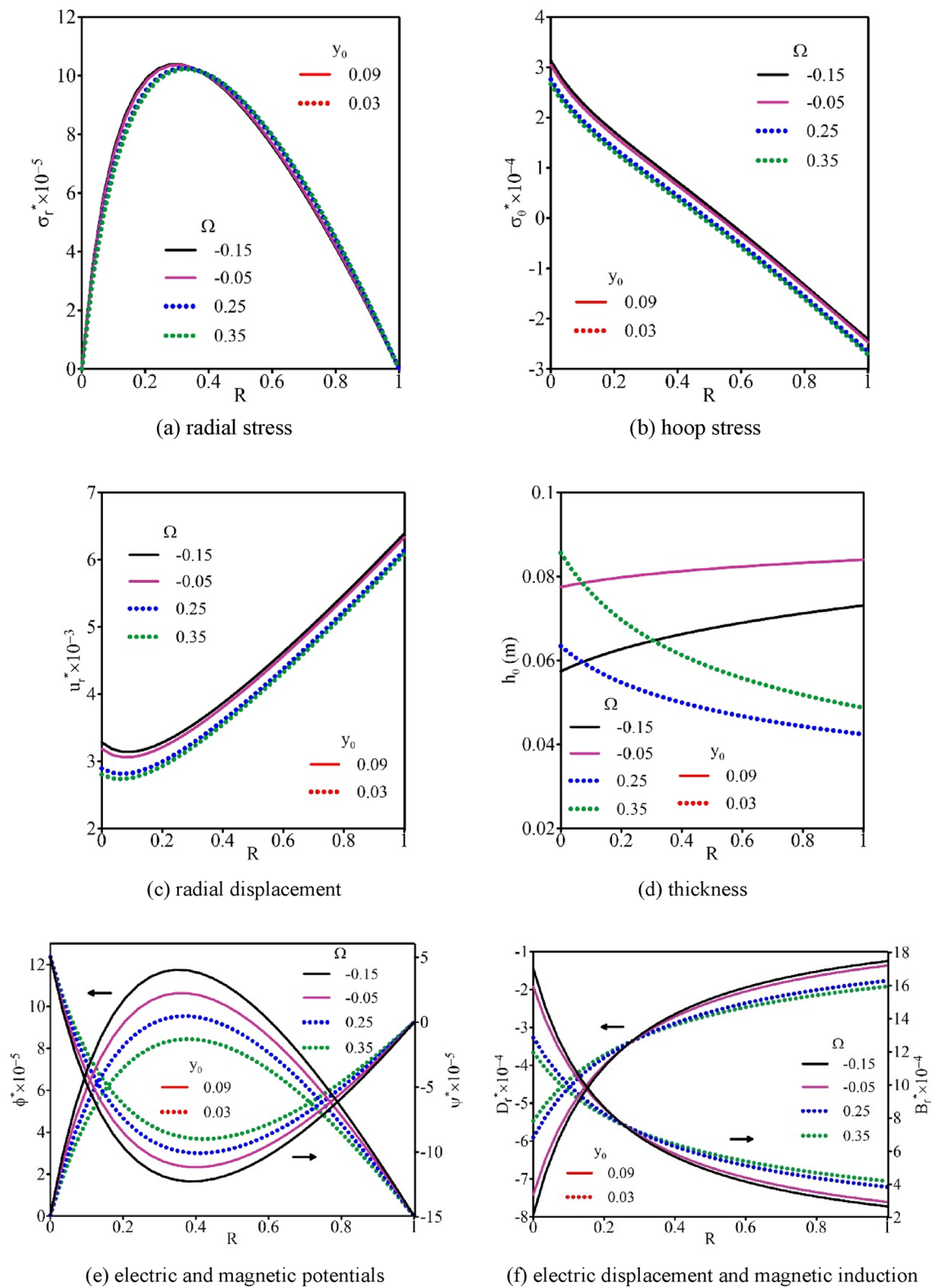
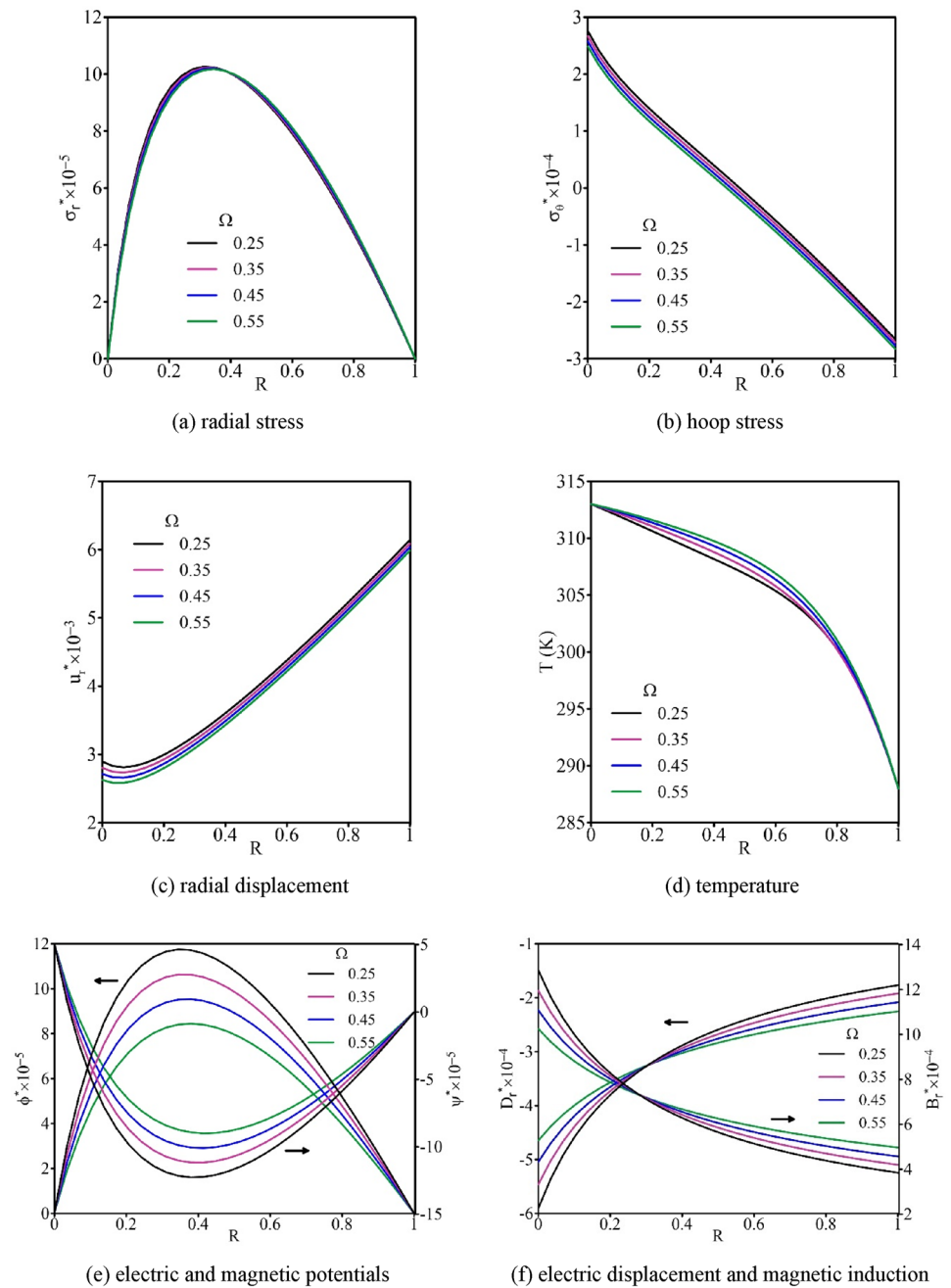


Fig. 5 Influence of the different profiles of thickness

Fig. 6 Influence of the thickness profile coefficient



examples are as Table 2. The following dimensionless parameters were used in the results:

$$R = \frac{r - r_i}{r_o - r_i}, \sigma_{r,\theta}^* = \frac{\sigma_{r,\theta}}{c_{11}}, u_r^* = \frac{u_r}{r_i}, \phi^* = \frac{\phi \sqrt{\beta_{11}/c_{11}}}{r_o},$$

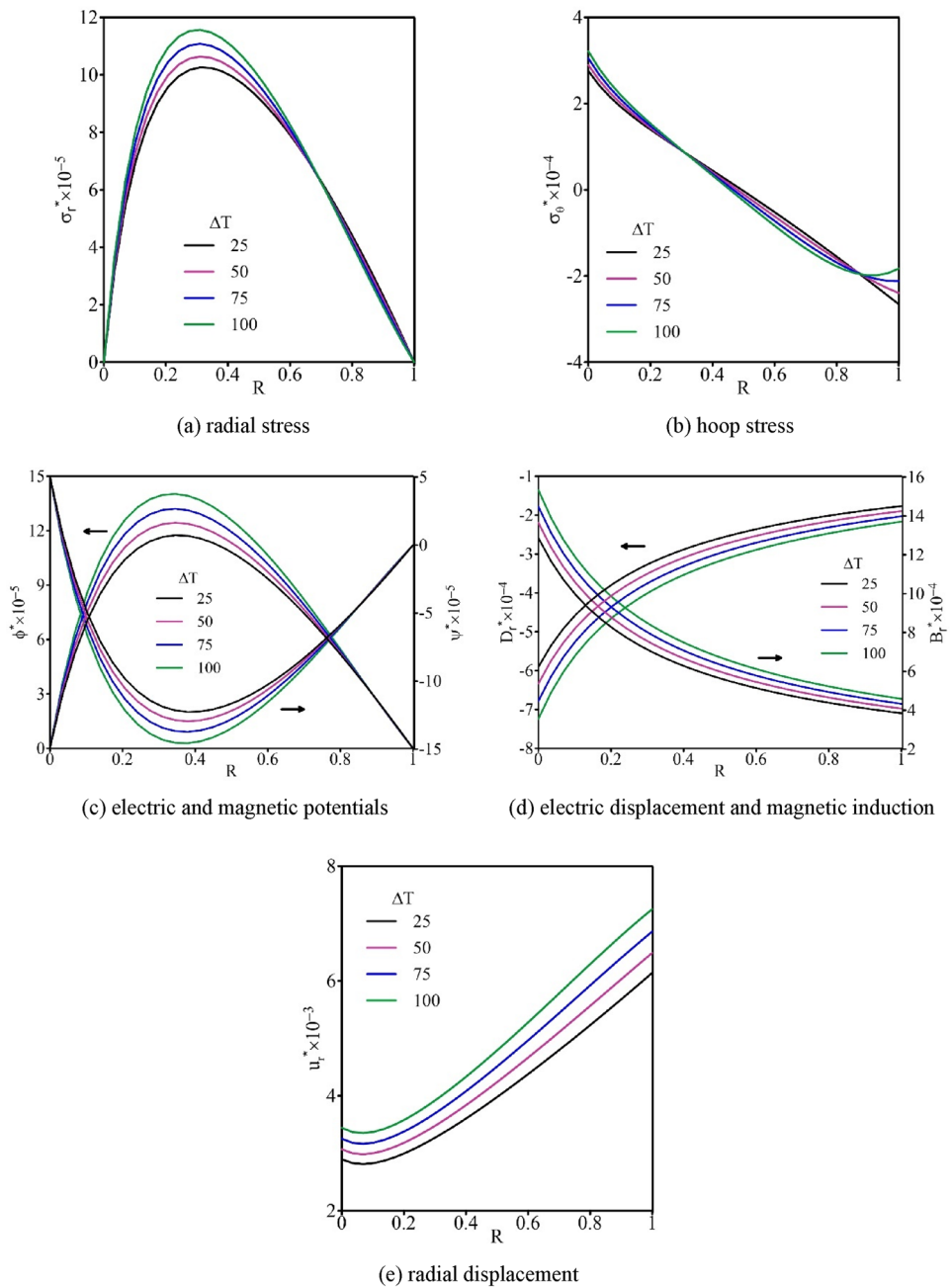
$$\psi^* = \frac{\psi \sqrt{d_{11}/c_{11}}}{r_o}, D_r^* = \frac{D_r}{\sqrt{c_{33}\epsilon_{11}}}, B_r^* = \frac{B_r}{\sqrt{c_{33}\mu}}. \tag{52}$$

4.1 Validation

4.1.1 Thermal Analysis

Since there are no comparable results in the literature, to validate the accuracy of the solution method used for the heat transfer equation, a numerical solution was performed using the FlexPDE software for the heat transfer equation. According to Fig. 2, the results show good agreement.

Fig. 7 Influence of the temperature difference



4.1.2 Stress Analysis

The obtained results for radial stress, hoop stress and radial displacement of the FGMEE disk were compared with the reported research about static behaviors of an FGM disk. The used material constants are listed in Refs. (Çallioğlu et al. 2011) and (Dai and Dai 2016). The obtained results have a good accuracy according to Fig. 3.

4.2 Effective Parameters Investigation

The influences of key parameters on the radial and circumferential stresses, radial deformation, electric and magnetic potentials, and temperature were analyzed in this section.

4.2.1 Grading Index

The inhomogeneity index is the first parameter to disclose its influence. Figure 4 illustrates the effects of the inhomogeneity index on the response of the disk. As shown, the outward radial displacement, radial stress, absolute hoop stress, and temperature reduce by an increase in the inhomogeneity index, whereas the electric potential and magnetic potential increase for a higher grading index. So, by selecting the proper grading index, the stress and displacement can be controlled.

4.2.2 Different Profiles of Thickness

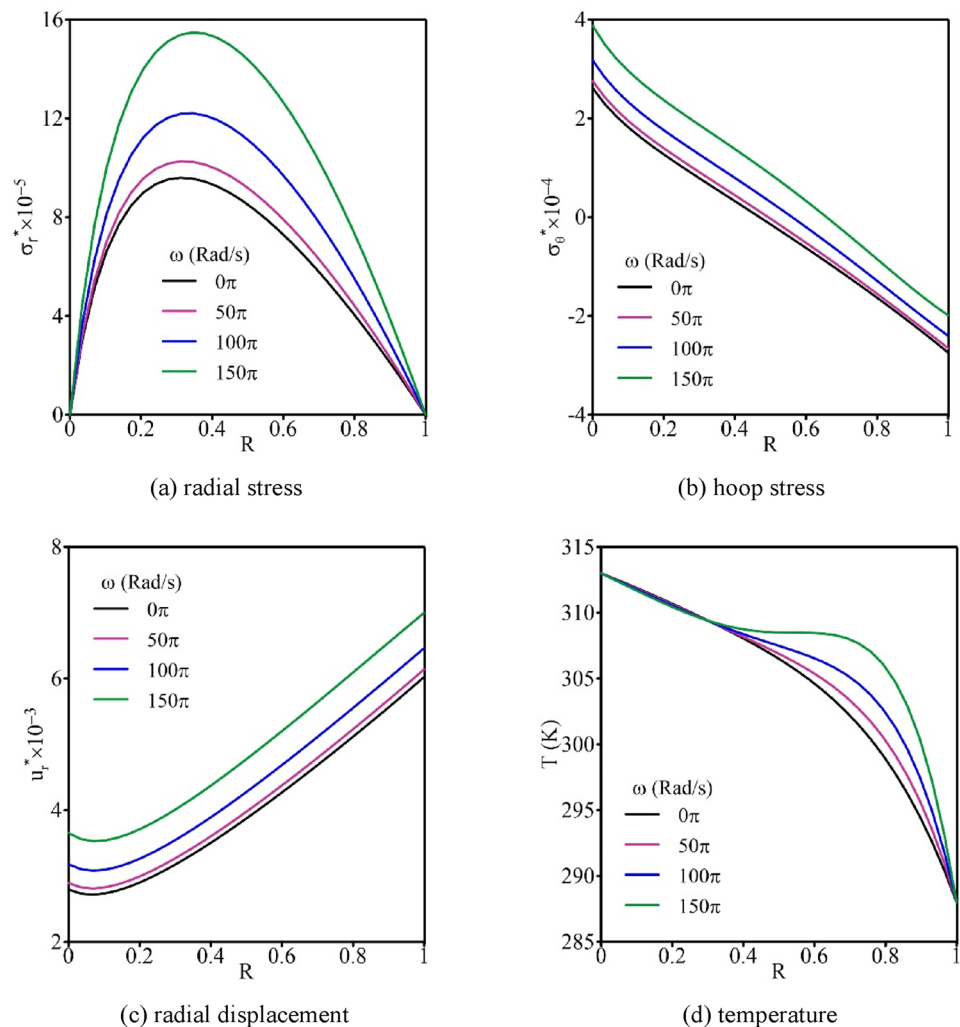
For the next example, the effect of the inner and outer thickness of the disk was disclosed. The findings can be observed in Fig. 5. Regarding Fig. 5, the outward displacement, electric potential, magnetic potential, maximum of electric displacement, and maximum of magnetic induction are smaller

for the case $h_o < h_i$ comparison with the case $h_o > h_i$. Also, the positive circumferential stress at the interior radius has a smaller value, and negative hoop stress at the exterior radius has a higher absolute value for the case $h_o < h_i$ comparison with the case $h_o > h_i$. It should be noted that FGMEEs usually have brittle behavior. So, high tensile hoop stress can increase the chance of crack growth and must be avoided. Also, the graphs show that changes in the inner and outer thickness have a slight effect on the radial stress. Generally, Fig. 5 shows that using a non-uniform thickness disk with an outer thickness smaller than the inner thickness can reduce the radial displacement, maximum tensile hoop stress, and electromagnetic potentials.

4.2.3 Thickness Coefficient

The changes in the stresses, radial displacement, and electromagnetic potentials for different thickness coefficients were investigated in this example. Figure 6 shows a higher value

Fig. 8 Effect of the angular velocity



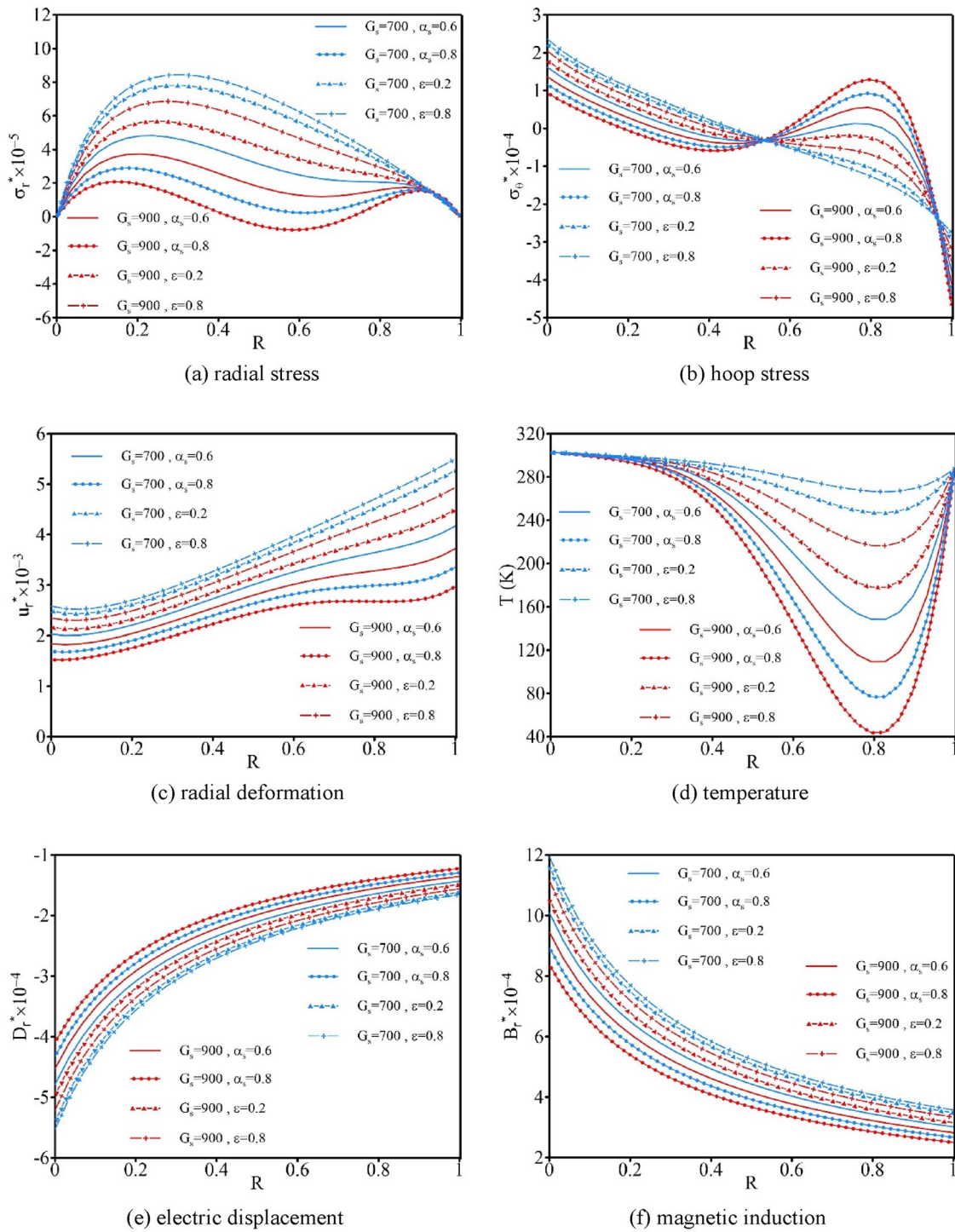


Fig. 9 Effect of solar radiation coefficients on the temperature distributions

of the thickness coefficient leads to a reduction in radial displacement, electric potential, magnetic potential, electric displacement, and magnetic induction. Also, the graph of

hoop stress shifts down for a higher thickness coefficient. As shown, the radial stress shows no significant change for different thickness coefficients. Moreover, the temperature

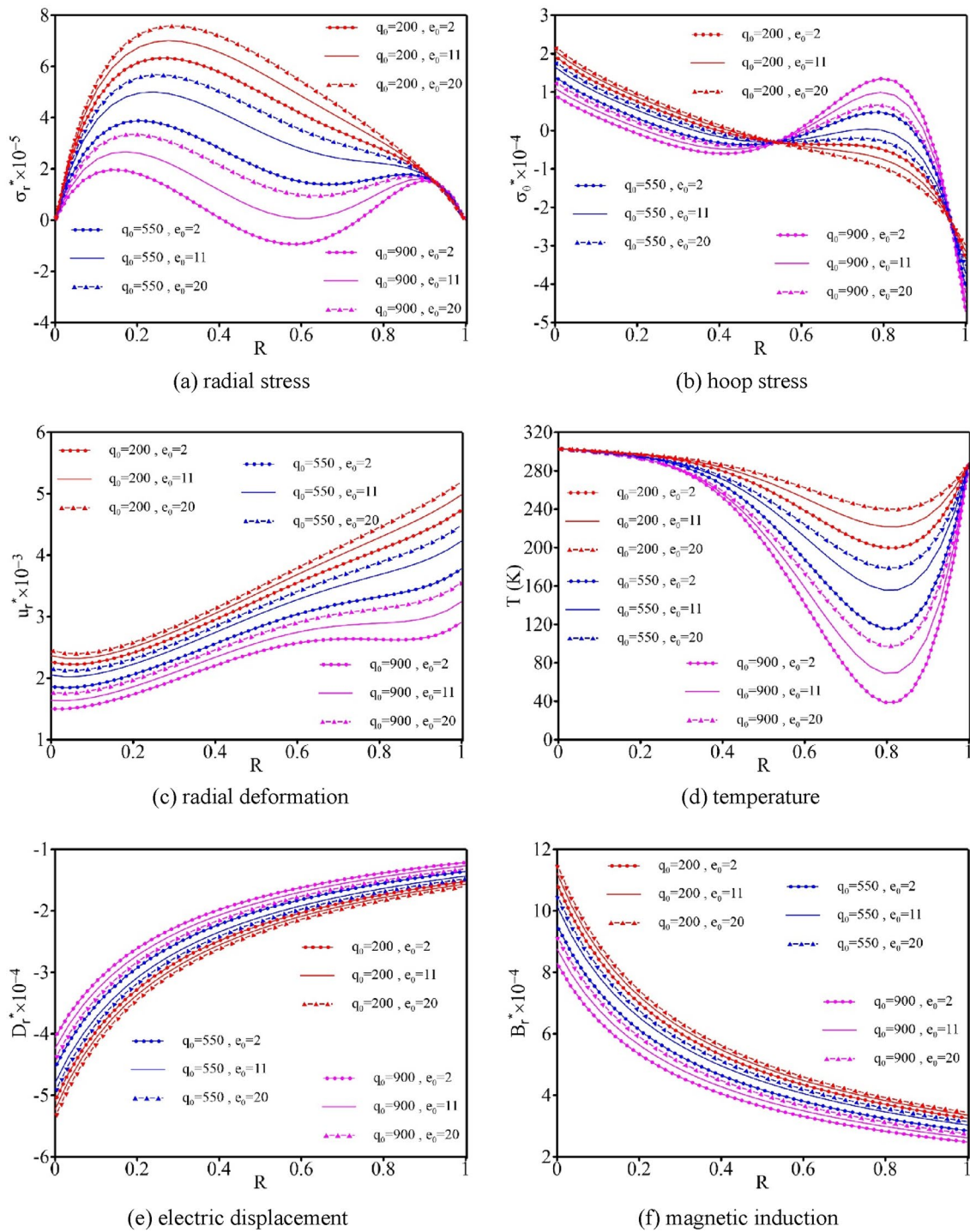


Fig. 10 Effect of internal heat generation coefficients on the temperature distributions

increases at the same radius for a higher thickness index. It should be noted that higher thickness coefficients mean disks with thicker thickness.

4.2.4 Temperature Difference

In the next example, the effect of temperature difference was explored. Figure 7 shows the influence of the temperature

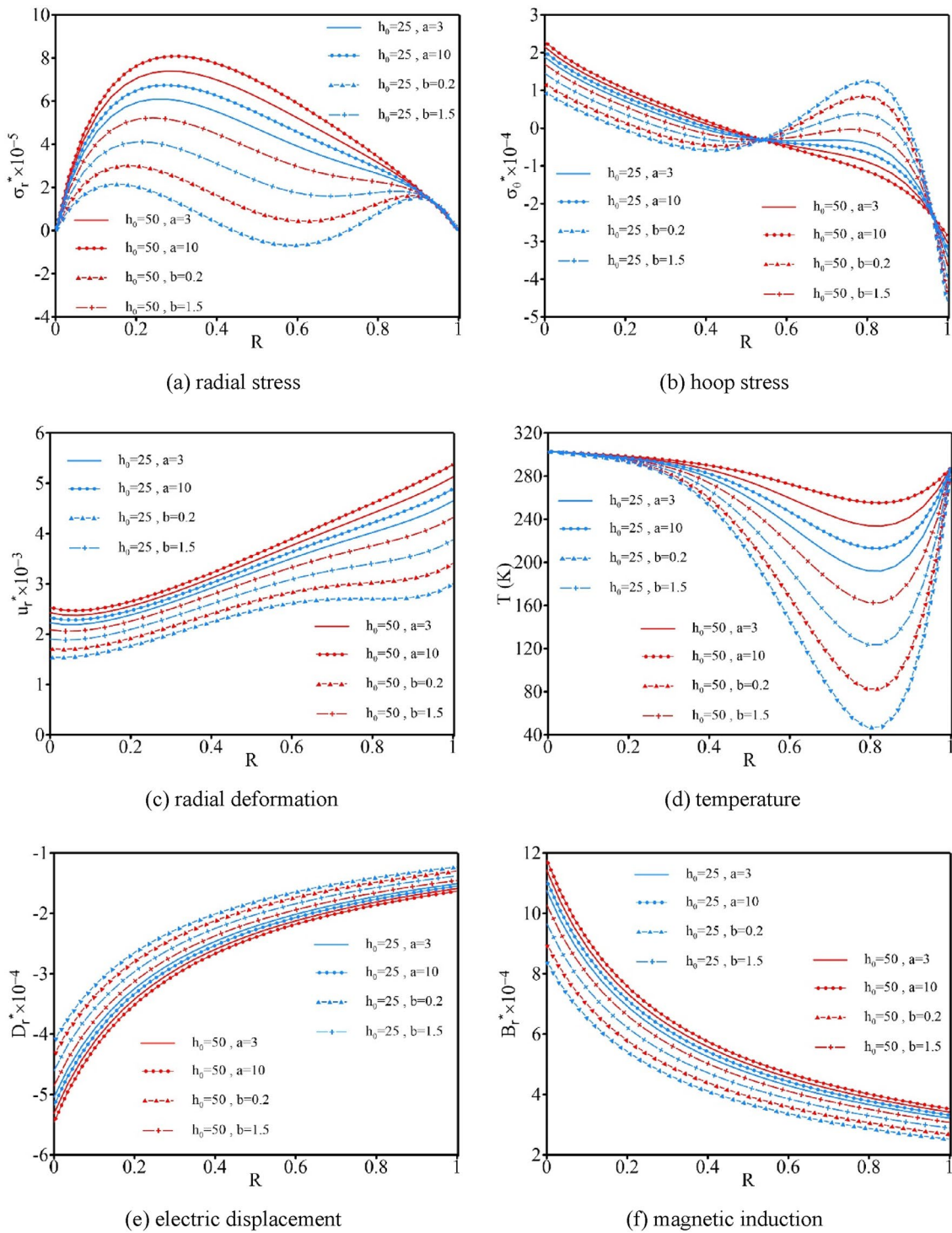


Fig. 11 Effect of convection heat transfer coefficients on the temperature distributions

difference between the inside and outside of the disk on stresses, displacement, electric and magnetic potentials, and electric and magnetic displacement. As shown, the radial stress, outward deformation, electric potential, magnetic

potential, electric displacement, and magnetic induction increase for the higher temperature difference. Moreover, there are two points through the thickness in which the circumferential stress shows no change by a change in

temperature difference. The trend of changes before and after these two points is in contrast with the trend of changes between them. Also, the maximum tensile circumferential stress increases for a higher temperature difference.

4.2.5 Angular Velocity

Figure 8 indicates the influence of the angular speed on the stress behavior of the disk. As observed, higher angular speed results in higher radial stress and deformation. The rate of change is incremental. Also, the tensile hoop stress at the interior radius increases, and compressive circumferential stress at the exterior radius decreases for higher angular speed. Since these smart materials show brittle behavior, a high tensile circumferential stress can yield crack growth. So, the high tensile hoop stress must be avoided. In addition, in the second half of thickness, the temperature graph shows an increase in temperature for a higher angular speed. It should be noted that the convection heat transfer is a function of angular velocity according to Eq. (4). Therefore, this effect is observed due to the effect of convection heat transfer.

4.2.6 Solar Radiation

For the next parameter, changes in the mechanical response due to solar radiation are illustrated in Fig. 9. Here, we have: $T_b = 303(\text{K})$, $T_o = 288(\text{K})$, $k_0 = 4.5(\text{W/mK})$, $h_0 = 0$, $\omega = 20\pi(\text{Rad/s})$, and $\beta = 3$. The graph shows that the tensile radial stress, radial deformation, electric displacement, and magnetic induction decrease for higher values for coefficients G_s and α_s . Also, it results in more reduction in the temperature distribution graph. However, the coefficient ε exhibits an opposite effect on stresses, displacement, temperature, electric displacement, and magnetic induction. Besides, there exist two points in which the circumferential stress is independent of solar radiation. Also, the location of maximum hoop stress changes from inside radius to a point between these two fixed points for higher values for coefficients G_s and α_s .

4.2.7 Internal Heat Generation

The effects of the internal heat source were disclosed in the next example. Here, we have: $T_b = 303(\text{K})$, $T_o = 288(\text{K})$, $k_0 = 4.5(\text{W/mK})$, $h_0 = 0$, $\omega = 20\pi(\text{Rad/s})$, and $\beta = 3$. The internal heat generation is temperature dependent according to Eq. (5). So, the power of the heat source depends on two parameters q_0 and e_0 that are investigated in Fig. 10. Concerning Fig. 10, the tensile radial stress, radial deformation, electric displacement, and magnetic induction decrease for higher source powers. Moreover,

the location of maximum tensile hoop stress changes from the inside radius to a radius through the thickness. Also, more reduction can be observed in the temperature distribution for the higher values of source power. According to Fig. 10, the temperature dependency coefficient e_0 has reverse effects in comparison with power source q_0 .

4.2.8 Convection Heat Transfer

The influence of convection heat transfer was disclosed in this part. In this case, we have: $T_b = 303(\text{K})$, $T_o = 288(\text{K})$, $k_0 = 4.5(\text{W/mK})$, $\varepsilon = 0.1$, $\alpha_s = 0.8$, and $\beta = 3$. According to Eq. (4), the convection heat transfer constant is temperature-dependent, and it depends on three parameters h_0 , b , and a . The effects of these constants are indicated in Fig. 11. According to Fig. 11, the radial stress, outward deformation, electric displacement, and magnetic induction increase for the higher values of h_0 , a , and b . Also, it results in an increase in the maximum tensile hoop stress at the inner radius. Furthermore, less reduction can be observed in the temperature distribution for the higher values of h_0 , a , and b .

4.2.9 Conduction Heat Transfer

The effect of heat conduction constant and heat conduction temperature dependency should be investigated in the next example. Here, $T_b = 303(\text{K})$, $T_o = 288(\text{K})$, $h_0 = 0$, $\varepsilon = 0.1$, and $\alpha_s = 0.8$. According to Eq. (3), the thermal conductivity constant is temperature-dependent, and it depends on two constants k_0 and β . Figure 12 shows the effects of these two constants. As observed, the tensile radial stress, radial displacement, electric displacement, and magnetic induction increase for a higher conductivity constant k_0 . Besides, the location of maximum hoop stress changes from a point through the thickness to the interior radius for a higher conductivity constant. Also, less reduction can be observed in the temperature distribution graph for the higher values of the conductivity constant. Figure 12 indicates that the effects of temperature dependency constant β are opposite to the effects of conductivity constant k_0 .

5 Conclusions

The thermoelastic response of a rotating functionally graded magneto-electro-elastic disk with non-constant thickness was investigated considering internal heat generation, convection, and radiation heat transfer. The heat conduction and convection coefficients are functions of temperature and radius. The differential transformation method was used for solving the obtained nonlinear differential equation of

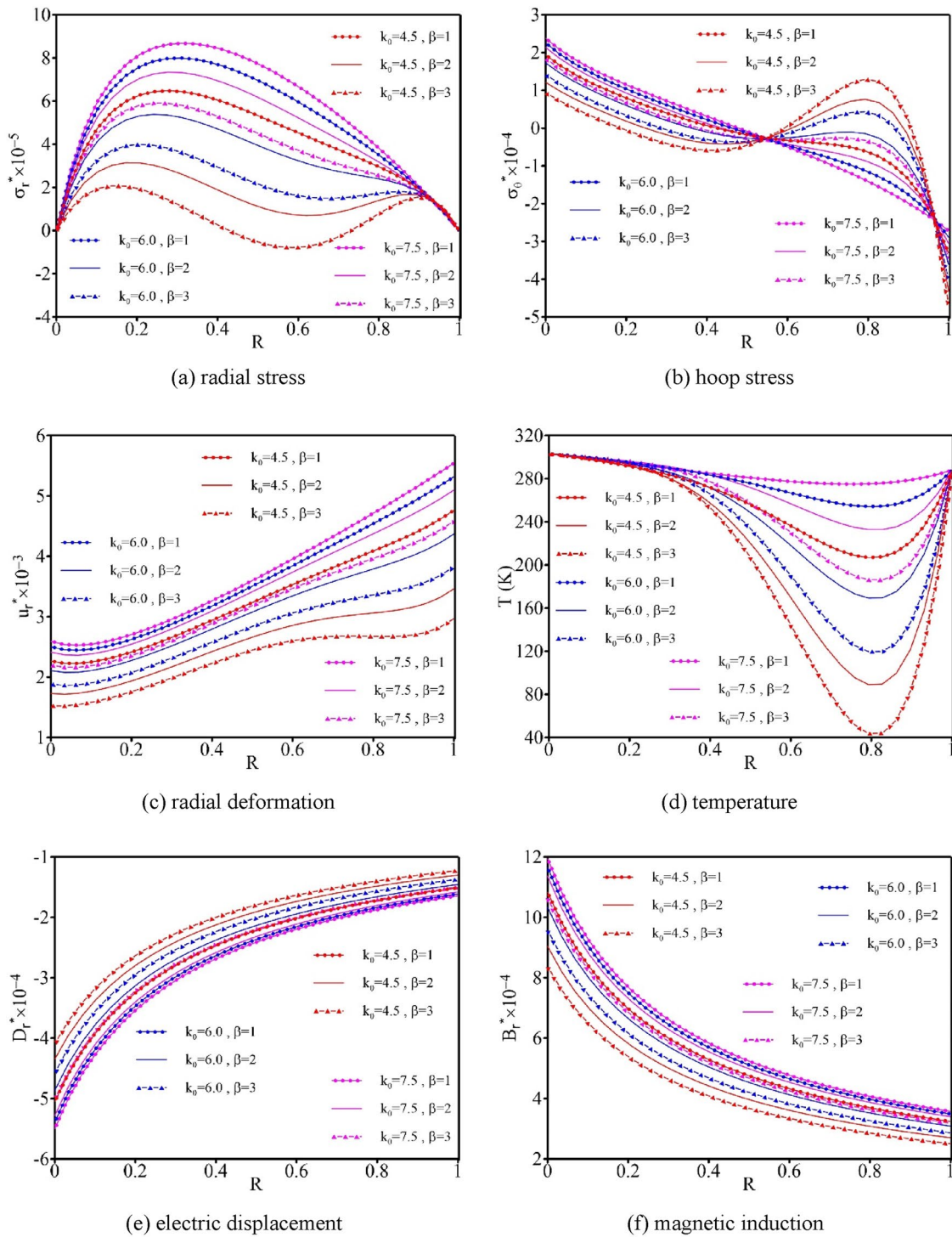


Fig. 12 Effect of conduction heat transfer coefficients on the temperature distributions

heat transfer. Then, the equilibrium equation of the disk was derived and solved analytically. The radial stress, circumferential stress, radial deformation, electric and magnetic potential, electric displacement, and magnetic induction can

be obtained. The following findings can be expressed based on the results:

- The displacement, radial stress, absolute hoop stress, and temperature reduce by an increase in the inhomogeneity

Table 3 Changing functions in the DTM method

Original function	Transformed function
$z(y) = u(y) \pm v(y)$	$Z(k) = U(k) \pm V(k)$
$z(y) = \beta u(y)$	$Z(k) = \beta U(k)$
$z(y) = \frac{d^n u(y)}{dy^n}$	$Z(k) = (k+1)(k+2)\dots(k+n)U(k+n)$
$z(y) = u(y)v(y)$	$Z(k) = \sum_{r=0}^k V(r)U(k-r)$
$z(y) = y^n$	$Z(k) = \delta(k-n); \delta(k-n) = \begin{cases} 1 & k = n \\ 0 & k \neq n \end{cases}$
$z(y) = \exp(\eta y)$	$Z(k) = \frac{\eta^k}{k!}$
$z(y) = (1+y)^n$	$Z(k) = \frac{n(n-1)\dots(n-k+1)}{k!}$
$z(y) = \sin(\Omega y + \beta)$	$Z(k) = \frac{\Omega^k}{k!} \sin\left(\frac{\pi k}{2} + \beta\right)$
$z(y) = \cos(\Omega y + \beta)$	$Z(k) = \frac{\Omega^k}{k!} \cos\left(\frac{\pi k}{2} + \beta\right)$
$z(y) = \int_{y_0}^y u(t)dt$	$Z(k) = \frac{U(k-1)}{k}, k \geq 1, Z(0) = 0$

index, whereas the electric potential and magnetic potential increase for the higher grading indexes.

- Using a non-uniform thickness disk with an outer thickness smaller than the inner thickness can reduce the radial displacement, maximum tensile hoop stress, and electromagnetic potentials.
- The radial stress, displacement, electric and magnetic potentials, electric displacement, and magnetic induction increase for the higher temperature difference.
- The tensile radial stress, radial deformation, electric displacement, and magnetic induction decrease for higher values of coefficients of solar flux intensity and absorption coefficient of solar radiation. However, the emission coefficient exhibits an opposite effect.
- The tensile radial stress, radial deformation, electric displacement, and magnetic induction decrease for higher source powers. Also, the location of maximum tensile hoop stress changes from the inside radius to a radius through the thickness. The temperature dependency coefficient has reverse effects in comparison with the power source.
- The radial stress and displacement, electric displacement, and magnetic induction increase for the higher values of the convection coefficients.
- The tensile radial stress, radial displacement, electric displacement, and magnetic induction increase for a higher conductivity constant. Also, the location of maximum hoop stress changes from a point through the thickness to the interior radius for a higher conductivity constant. The effects of the temperature-dependency constant are opposite to the effects of the conductivity constant.

Appendix

The basic functions used in the DTM are defined as (Zhou 1986; Chen and Ho 1996):

See Table 3.

Funding The author received no financial support for the research, authorship, and/or publication of this article.

Declarations

Conflict of interest The authors declare that they have no conflict of interest.

References

- Ahmad S (2023) Computational analysis of comparative heat transfer enhancement in Ag-H₂O, TiO₂-H₂O and Ag-TiO₂-H₂O: finite difference scheme. *J Taiwan Inst Chem Eng* 142:104672
- Ahmad S, Hayat T, Alsaedi A, Khan Z, Khan MW (2019) Finite difference analysis of time-dependent viscous nanofluid flow between parallel plates. *Commun Theor Phys* 71:1293–1300
- Ahmad S, Hayat T, Alsaedi A (2021a) Computational analysis of entropy generation in radiative viscous fluid flow. *J Therm Anal Calorim* 143(3):2665–2677
- Ahmad S, Hayat T, Alsaedi A, Ullah H, Shah F (2021b) Computational modeling and analysis for the effect of magnetic field on rotating stretched disk flow with heat transfer. *Propul Power Res* 10(1):48–57
- Akbarzadeh A, Chen Z (2012) Magneto-electroelastic behavior of rotating cylinders resting on an elastic foundation under hygrothermal loading. *Smart Mater Struct* 21(12):125013
- Alibeigloo A (2021) Transient response analysis of sandwich cylindrical panel with FGM core subjected to thermal shock. *Int J Mech Mater Design* 17:707–719
- Bose T, Rattan M (2018) Effect of thermal gradation on steady state creep of functionally graded rotating disc. *Eur J Mech-A/Solids* 67:169–176
- Çallioğlu H, Bektaş NB, Sayer M (2011) Stress analysis of functionally graded rotating discs: analytical and numerical solutions. *Acta Mech Sin* 27(6):950–955
- Chang D-M, Liu X-F, Wang B-L, Liu L, Wang T-G, Wang Q, Han J-X (2020) Exact solutions to magneto-electro-thermo-elastic fields for a cracked cylinder composite during thermal shock. *Int J Mech Mater Design* 16:3–18
- Chen C-K, Ho S-H (1996) Application of differential transformation to eigenvalue problems. *Appl Math Comput* 79(2–3):173–188
- Dai T, Dai H-L (2016) Thermo-elastic analysis of a functionally graded rotating hollow circular disk with variable thickness and angular speed. *Appl Math Model* 40(17):7689–7707
- Dai T, Dai H-L (2017) Analysis of a rotating FGME circular disk with variable thickness under thermal environment. *Appl Math Model* 45:900–924
- Dai H-L, Zheng Z-Q, Dai T (2017) Investigation on a rotating FGPM circular disk under a coupled hygrothermal field. *Appl Math Model* 46:28–47
- Dai T, Dai H-L, Lin Z-Y (2019) Multi-field mechanical behavior of a rotating porous FGME circular disk with variable thickness under hygrothermal environment. *Compos Struct* 210:641–656
- Ebrahimi F, Jafari A, Mahesh V (2019) Assessment of porosity influence on dynamic characteristics of smart heterogeneous

- magneto-electro-elastic plates. *Struct Eng Mech Int'l J* 72(1):113–129
- Eldeeb AM, Shabana YM, Elsawaf A (2021) Influences of angular deceleration on the thermoelastoplastic behaviors of nonuniform thickness multilayer FGM discs. *Compos Struct* 258:113092
- Gupta V, Singh S (2016) Mathematical modeling of creep in a functionally graded rotating disc with varying thickness. *Regener Eng Transl Med* 2(3):126–140
- Hayat T, Ahmad S, Khan MI, Alsaedi A (2018) Modeling and analyzing flow of third grade nanofluid due to rotating stretchable disk with chemical reaction and heat source. *Physica B* 537:116–126
- Hosseini M, Shishesaz M, Tahan KN, Hadi A (2016) Stress analysis of rotating nano-disks of variable thickness made of functionally graded materials. *Int J Eng Sci* 109:29–53
- Hosseini M, Shishesaz M, Hadi A (2019) Thermoelastic analysis of rotating functionally graded micro/nanodisks of variable thickness. *Thin-Walled Struct* 134:508–523
- Incropera FP, DeWitt DP, Bergman TL, Lavine AS (1996) Fundamentals of heat and mass transfer. Wiley, New York
- Kaur H, Gupta N, Singh SB (2020) Effect of thermal gradient on the deformation of a rotating composite disk. *Mater Today: Proc* 26:3363–3368
- Khanna K, Gupta VK, Nigam SP (2017) Creep Analysis in Functionally Graded Rotating Disc Using Tresca Criterion and Comparison with Von-Mises Criterion. *Mater Today: Proc* 4(2, Part A):2431–2438
- Khorsand M, Tang Y (2018) Design functionally graded rotating disks under thermoelastic loads: weight optimization. *Int J Press Vessels Pip* 161:33–40
- Li G, Li Y, Bao M, Ding S (2019) Experimental study of thermal loading management strategy for the transient process of a rotating turbine disk. *Exp Thermal Fluid Sci* 103:234–246
- Ly D, Nguyen-Thoi T, Truong-Thi T, Nguyen Sy N (2022) Multi-objective optimization of the active constrained layer damping for smart damping treatment in magneto-electro-elastic plate structures. *Int J Mech Mater Design* 18:633–663
- Madan R, Bhowmick S, Nath Saha K (2018) Stress and deformation of functionally graded rotating disk based on modified rule of mixture. *Mater Today: Proc* 5(9, Part 3):17778–17785
- Madan R, Bhowmick S, Saha K (2019) Limit angular speed of L-FGM rotating disk for both temperature dependent and temperature independent mechanical properties. *Mater Today: Proc* 18:2366–2373
- Rattan M, Kaushik A, Chamoli N, Bose T (2016) Steady state creep behavior of thermally graded isotropic rotating disc of composite taking into account the thermal residual stress. *Eur J Mech A Solids* 60:315–326
- Saadatfar M (2019) Analytical solution for the creep problem of a rotating functionally graded magneto–electro–elastic hollow cylinder in thermal environment. *Int J Appl Mech* 11(06):1950053
- Saadatfar M (2021a) Multiphysical time-dependent creep response of FGME hollow cylinder in thermal and humid environment. *Mech Time-Depend Mater* 25(2):151–173
- Saadatfar M (2021) Transient response of a hollow functionally graded piezoelectric cylinder subjected to coupled hygrothermal loading. *Int J Appl Mech* 13:2150109
- Saadatfar M, Zarandi MH (2020) Deformations and stresses of an exponentially graded magneto-electro-elastic non-uniform thickness annular plate which rotates with variable angular speed. *Int J Appl Mech* 12:2050050
- Saadatfar M, Zarandi MH (2020b) Effect of angular acceleration on the mechanical behavior of an exponentially graded piezoelectric rotating annular plate with variable thickness. *Mech Based Des Struct Mach* 50:1–17
- Saadatfar M, Zarandi M, Babaelahi M (2021) Effects of porosity, profile of thickness, and angular acceleration on the magneto-electro-elastic behavior of a porous FGME rotating disc placed in a constant magnetic field. *Proc Inst Mech Eng C J Mech Eng Sci* 235(7):1241–1257
- Saadatfar M, Babazadeh MA, Babaelahi M (2023) Creep analysis in a rotating variable thickness functionally graded disc with convection heat transfer and heat source. *Mech Time-Depend Mater*. <https://doi.org/10.1007/s11043-023-09613-z>
- Saadatfar M, Babazadeh MA, Babaelahi M (2023) Stress and deformation of a functionally graded piezoelectric rotating disk with variable thickness subjected to magneto-thermo-mechanical loads including convection and radiation heat transfer. *Int J Appl Mech*. <https://doi.org/10.1142/S1758825124500029>
- Saber E, Abd_Elsalam A (2022) A Theoretical model for investigating the thermo-mechanical performance of functionally graded rotating discs with varying grading index values. *Forces in Mechanics* 8:100103
- Sahni M, Sahni R (2015) Rotating functionally graded disc with variable thickness profile and external pressure. *Procedia Comput Sci* 57:1249–1254
- Singh S, Harsha S (2020) Thermal buckling of porous symmetric and non-symmetric sandwich plate with homogenous core and S-FGM face sheets resting on Pasternak foundation. *Int J Mech Mater Design* 16:707–731
- Sondhi L, Kumar Thawait A, Sanyal S, Bhowmick S (2020) Stress and deformation analysis of functionally graded varying thickness profile orthotropic rotating disk. *Mater Today: Proc* 33:5455–5460
- Thawait A, Sondhi L, Sanyal S, Bhowmick S (2017) Elastic analysis of functionally graded variable thickness rotating disk by element based material grading. *J Solid Mech* 9:650–662
- Zhang S-Q, Zhao Y-F, Wang X, Chen M, Schmidt R (2022) Static and dynamic analysis of functionally graded magneto-electro-elastic plates and shells. *Compos Struct* 281:114950
- Zhou J (1986) Differential transformation and its applications for electrical circuits. Huazhong University Press, Wuhan
- Zhou L, Yang H, Ma L, Zhang S, Li X, Ren S, Li M (2022) On the static analysis of inhomogeneous magneto-electro-elastic plates in thermal environment via element-free Galerkin method. *Eng Anal Boundary Elem* 134:539–552

Springer Nature or its licensor (e.g. a society or other partner) holds exclusive rights to this article under a publishing agreement with the author(s) or other rightsholder(s); author self-archiving of the accepted manuscript version of this article is solely governed by the terms of such publishing agreement and applicable law.